

Supporting information

MIL-91(Ti), a small pore Metal-Organic Framework which fulfils several criteria: an upscaled green synthesis, excellent water stability, high CO₂ selectivity and fast CO₂ transport

Virginie Benoit ^a, Renjith S. Pillai ^b, Angelica Orsi ^c, Périne Normand ^d, Hervé Jobic ^e, Farid Nouar ^f, Pierre Billemont ^d, Emily Bloch ^a, Sandrine Bourrelly ^a, Thomas Devic ^f, Paul A. Wright ^c, Guy De Weireld ^d, Christian Serre ^f, Guillaume Maurin ^{b,†}, Philip L. Llewellyn ^{a,†}

^a. *Aix-Marseille Univ., CNRS, MADIREL UMR 7246, 13397 Marseille, France.*

^b. *UMR-5253, Université Montpellier, CNRS, ENSCM, Place E. Bataillon, 34095 Montpellier cedex 05, France.*

^c. *Eastchem School of Chemistry, University of St. Andrews, Purdie Building, North Haugh, St Andrews, Fife KY16 9ST, United Kingdom.*

^d. *Service de Thermodynamique, Faculté Polytechnique, Université de Mons, Place du Parc 20, 7000 Mons, Belgium*

^e. *Institut de Recherches sur la Catalyse et l'Environnement de Lyon, CNRS, Université de Lyon, 2. Av. A. Einstein, 69626 Villeurbanne, France.*

^f. *Institut Lavoisier, UMR CNRS 8180, Université de Versailles St Quentin en Yvelines, Université Paris-Saclay, 45 avenue des Etats-Unis, Versailles, 78035, France.*

^g.

† Corresponding authors.

Table of contents

| | |
|--|----|
| 1. Reflux synthesis of MIL-91(Ti) and initial characterization | 3 |
| 1.1. Synthesis of the ligand | 3 |
| 1.2. Preparation of MIL-91[Ti] from reflux heating involved mixing (60 °C, 30 minutes) 3 | |
| 1.3. Capillary PXRD | 4 |
| 1.4 SEM image..... | 5 |
| 2. Characterization of MIL-91(Ti) prepared by hydrothermal and reflux synthesis methods..... | 6 |
| 2.1. Thermogravimetric analysis..... | 6 |
| 2.2. Nitrogen physisorption at 77K | 7 |
| 2.3. Water adsorption at 25°C | 8 |
| 2.4. Adsorption calorimetry at 30°C | 9 |
| 3. Adsorption gravimetry at 30°C on the MIL-91(Ti) sample obtained by hydrothermal synthesis, Synchrotron PXRD during CO ₂ adsorption, and comparison with molecular simulations..... | 11 |
| 3.1. Adsorption gravimetry | 11 |
| 3.2. Synchrotron PXRD during CO ₂ adsorption | 12 |
| 3.3. Comparison of the adsorption properties between different MOFs | 13 |
| 4. Mixture adsorption | 17 |
| 5. Quasi-Elastic neutron scattering measurements..... | 20 |
| 6. Molecular simulations | 20 |
| 6.1. Computational Methods..... | 20 |
| 6.2. GCMC Simulations..... | 23 |
| 6.3. Computational predictions | 24 |

1. Reflux synthesis of MIL-91(Ti) and initial characterization

1.1. Synthesis of the ligand

The ligand N,N'-piperazinebis(methylenephosphonic acid) was synthesised from a modified Mannich reaction. ^[1] A mixture of hydrochloric acid (10 mL, 37 wt. %) and water (10 mL) was added to piperazine (6.89 g, 0.08 mol) and phosphorous acid (17.06 g, 0.21 mol) to form a colourless solution, which was then refluxed (1 hour). Formaldehyde (20 mL, 37 wt. %) was added drop wise over a 2 hour period to form a white suspension. After refluxing for 24 hours, the reaction was cooled and the solvent volume reduced by 70% under vacuum. An ethanol-water (9:1, 40 mL) solution was added to the product and refrigerated overnight to precipitate any remaining ligand. The product was collected by filtration, washed with an ethanol-water (9:1, 2 × 30 mL) solution and dried (90 °C, overnight) to afford a white powder (19.5 g, 89 % yield based on piperazine). δ_H (500 MHz, D₂O/NaOH, Me₄Si) 3.13 (4H, broad s, CH₂) and 2.79 (8H, d, *J* 11.9 Hz, CH₂). δ_C (126 MHz, D₂O/NaOH, Me₄Si) 57.1 (C-1, CP, ¹*J*(C-P) 140.6 Hz) and 53.6 (C-2, CN, ³*J*(C-P) 8.5 Hz). δ_P (202 MHz, D₂O/NaOH, 85% H₃PO₄) 14.4 (t, ²*J*(P-H) 12.2 Hz).

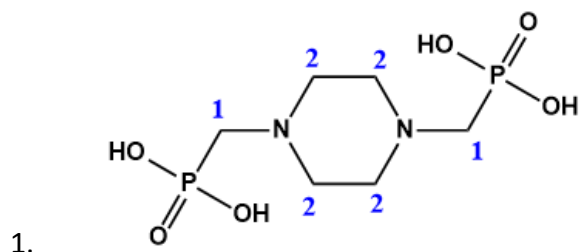


Figure S1. Numbered carbons of N,N'-piperazine(bismethylenephosphonic acid) ligand for ¹³C-NMR analysis.

1.2. Preparation of MIL-91[Ti] from reflux heating involved mixing (60 °C, 30 minutes)

N,N'-piperazinebis(methylenephosphonic acid) (1.14 g, 4.17 mmol) in water (30 mL) to produce an opaque white suspension. 1M NaOH was added drop wise to increase the pH to 5 or 6 and to partially dissolve the organic ligand. The mixture was further stirred (60 °C, 30 minutes). Titanium oxyacetylacetonate (1.09 g, 4.17 mmol) was then added as a dry powder

and a little water was added to rinse the sides of the reaction vessel. The temperature was increased to reflux (68 hours), cooled, filtered under gravity and washed with water (3 x 20 mL). The white precipitate (0.97 g, 55 % yield) was dried overnight (room temperature). Selected area EDX analysis resulted in Ti : P ratio (expected 1 : 2) of 1 : 1.9. Found: C, 19.6; H, 5.4; N, 7.5. Calc. for MIL-91[Ti] ($\text{TiO}_{10.6}\text{P}_2\text{C}_6\text{N}_2\text{H}_{23.2}$): C, 17.6; H, 5.7; N, 6.9 %.

1.3. Capillary PXRD

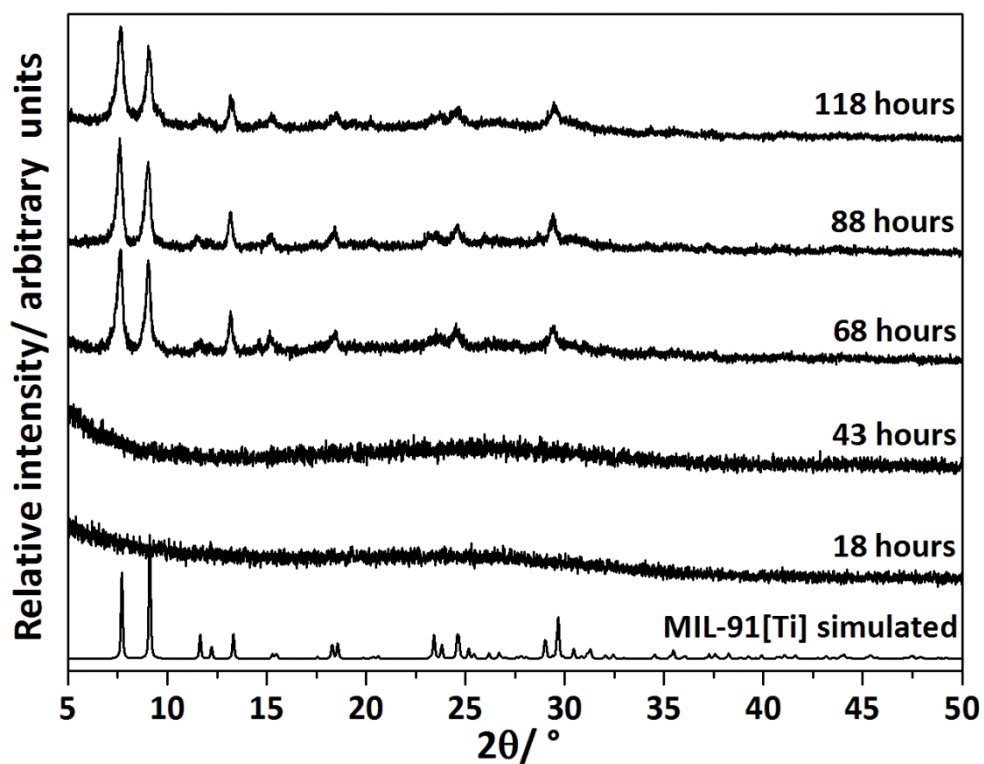


Figure S2. PXRD of samples taken periodically (after 18, 43, 68, 88, 118 hours) from an initial test run of the reflux solution.

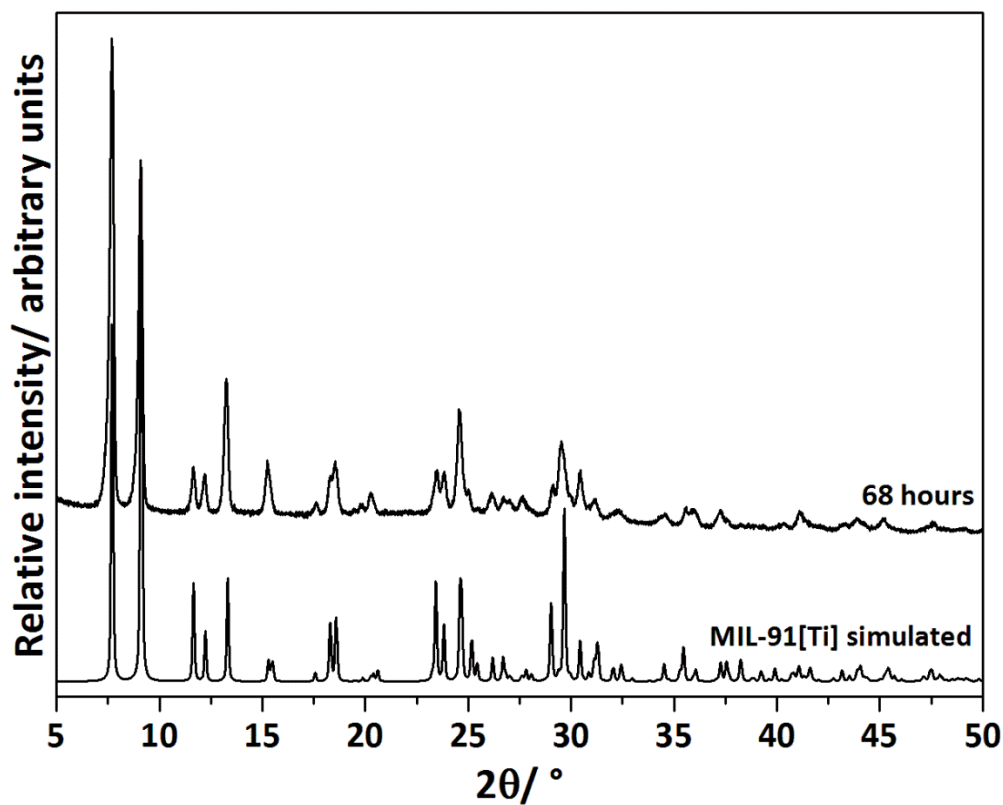


Figure S3. Overnight PXRD of MIL-91(Ti) reflux sample after 68 hours.

1.4 SEM image

Image S4 was obtained from the facility (FEGSEM Jeol JSM-6700F) at the University of St Andrews. The sample was sputter coated three times with gold in a Quorum Q150R ES (10 mA, 30 seconds and 2.3 tooling factor).

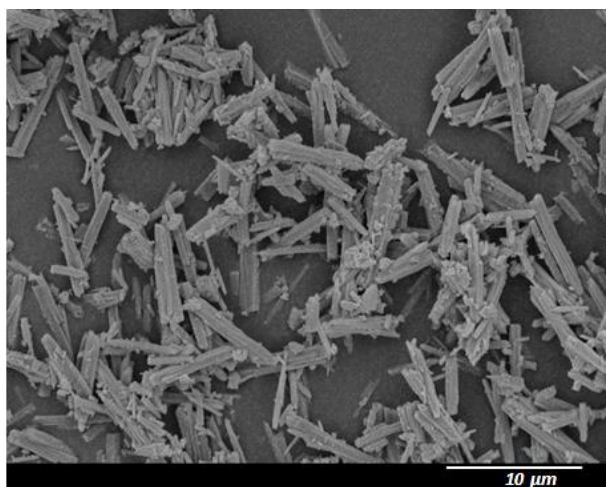


Image S4. SEM image of MIL-91[Ti] reflux sample after 68 hours.

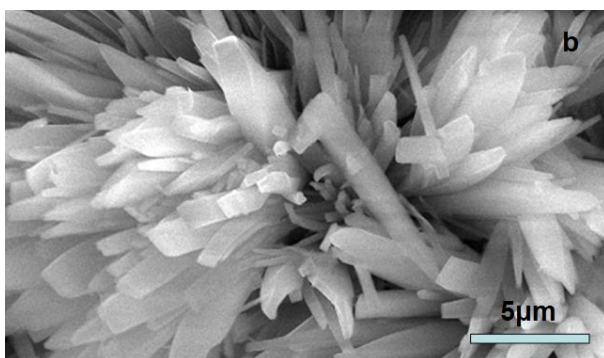


Image S5. SEM image of MIL-91[Ti] hydrothermal sample. (Courtesy of L. Gaberova, O. Schaef)

2. Characterization of MIL-91(Ti) prepared by hydrothermal and reflux synthesis methods

2.1. Thermogravimetric analysis

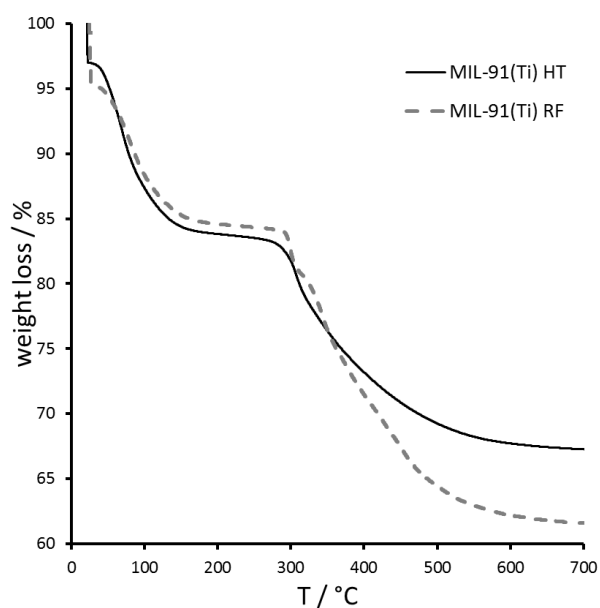


Figure S6. Thermogravimetric analysis of MIL-91(Ti) samples prepared under hydrothermal (HT) and reflux (RF) conditions.

The thermogravimetric analysis was carried out with a Q500 (TA Instruments) under air flow (100 mL/min) with a linear heating rate of 5 K / min (Figure S6).

An initial isotherm at room temperature under gas flow allows external species, such as physisorbed water, to be removed. For both samples, two main mass losses can be observed. Up to 200°C, adsorbed species within the pores are removed (probably water, and any other solvents). Under these conditions above 300°C, structure degradation occurs.

2.2. Nitrogen physisorption at 77K

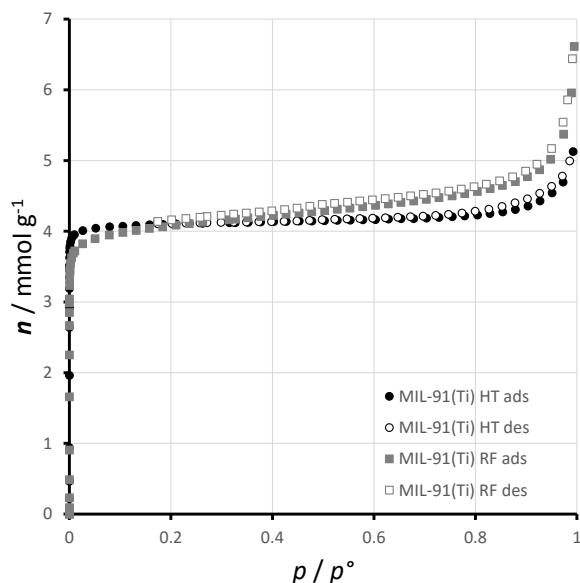


Figure S7. Nitrogen adsorption-desorption isotherms at 77 K obtained with MIL-91(Ti) samples prepared under hydrothermal (HT) and reflux (RF) conditions.

The nitrogen isotherms at 77 K (Figure S7) were obtained with a BelMAX apparatus (BEL Japan) after outgassing under secondary vacuum to 150°C. Both isotherms are of Type-I, indicative of microporosity.^[2] The BET method was used to estimate an equivalent BET area^[3] and the t-plot used to calculate the external surface area. This data analysis from these experiments is given in Table S1, below. It can be appreciated, in comparison with the data obtained from molecular modeling (Table S2), that maybe these samples could be improved in terms of activation to optimize the pore volume and BET area.

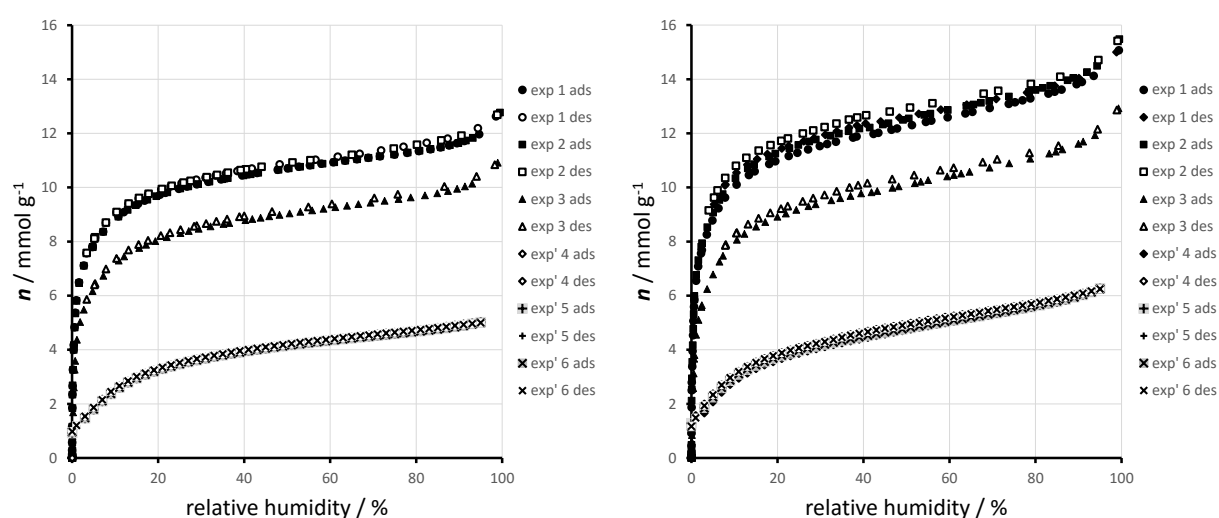
Table S1. Table of characteristics obtained from the nitrogen isotherms

| Sample | BET area / $\text{m}^2 \text{g}^{-1}$ | BET range (p/p°) | C value | t-plot external surface area / $\text{m}^2 \text{g}^{-1}$ | pore volume at $p/p^\circ=0.1$ / $\text{cm}^3 \text{g}^{-1}$ |
|--|---------------------------------------|---------------------------|---------|---|--|
| MIL-91(Ti) (hydrothermal synthesis) | HT 382 | 4.10^{-6} to 0.01 | 68000 | 7 | 0.141 |
| MIL-9-(Ti) (reflux synthesis) | RF 363 | 4.10^{-6} to 0.025 | 19000 | 23 | 0.138 |

Table S2. Pore diameter (\AA), BET area ($\text{m}^2 \text{g}^{-1}$), pore volume ($\text{cm}^3 \cdot \text{g}^{-1}$) calculated from the DFT-optimized crystal structures

| MIL91(Ti) | d_{pore} | S_{BET} | V_{pore} |
|------------|-------------------|------------------|-------------------|
| Simulation | 3.9 | 403 | 0.16 |

2.3. Water adsorption at 25°C

**Figure S8.** Water adsorption-desorption isotherms at 25°C obtained with MIL-91(Ti) samples prepared under hydrothermal (HT) (LEFT) and reflux (RF) (RIGHT) conditions.

Exp 1 was carried out after outgassing under secondary vacuum to 150°C. Exp 2 was a repeat experiment after again outgassing to 150°C. Exp 3 was carried out on the same sample after evacuation for 1 hour at 25°C. Exp' 4 was carried out on a fresh sample after outgassing to 80°C under nitrogen flow. Exp' 5 and exp'6 are repeated experiments after evacuation for 3 hours under nitrogen flow at 25°C

Two series of water adsorption experiments were carried out on the two MIL-91(Ti) samples (Figure S8). A first series of experiments (exp 1, exp 2 & exp 3) were carried out using the BelMAX apparatus (BEL Japan) after initially outgassing under secondary vacuum to 150°C. These experiments are described in the main text. A second series of experiments (exp' 4, exp' 5 & exp' 6) were carried out under nitrogen flow at 25°C (Q5000, TA Instruments) after an initial outgassing under nitrogen flow to 80°C. These last three experiments took around 3 weeks to complete and the fact that a complete overlap occurs suggests a certain level of stability to water. This stability is confirmed by the unchanged XRD pattern obtained with the sample obtained under reflux after the water adsorption-desorption cycles (Figure S9).

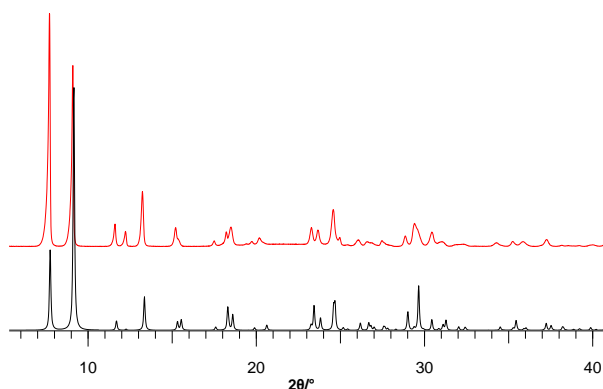


Figure S9. PXRD patterns of MIL-91(Ti) synthesised under reflux conditions (black, theoretical; red, after water adsorption cycling (over 3 weeks at 25°C) ($\lambda_{Cu} \sim 1.5406 \text{ \AA}$))

2.4. Adsorption calorimetry at 30°C

The microcalorimetry experiments were carried out at 303 K by means of a manometric dosing apparatus linked to the sample cell housed in a Tian-Calvet type microcalorimeter. ^[4] This apparatus allows the simultaneous measurement of the isotherm and corresponding differential enthalpies of adsorption up to a maximum pressure of 40 bar in the present

study. Around 0.3 g of sample was used for these experiments. An error of $\pm 1 \text{ kJ mol}^{-1}$ can be considered for these experiments. The gases used for the adsorption were obtained from Air Liquide and were of 99.998% purity or better. Prior to adsorption experiments, the samples were placed under a secondary vacuum and were heated to 150°C for 16 hours.

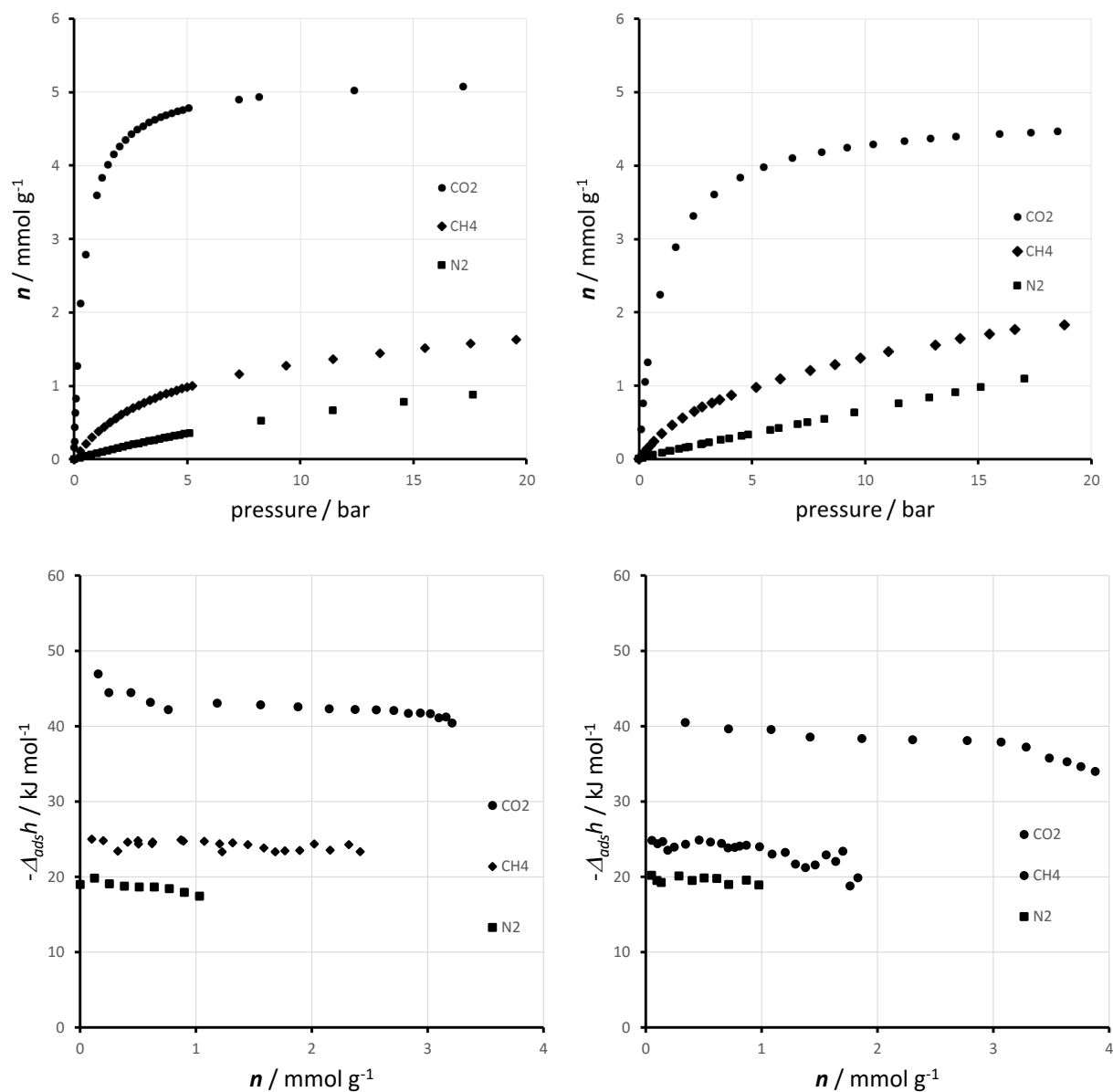


Figure S10. Comparison of the adsorption isotherms (top) and corresponding adsorption enthalpies as a function of the coverage collected by microcalorimetry (bottom) at 303 K for CO₂, CH₄, N₂ in MIL-91(Ti) prepared by hydrothermal synthesis (left) and reflux protocol (right).

3. Adsorption gravimetry at 30°C on the MIL-91(Ti) sample obtained by hydrothermal synthesis, Synchrotron PXRD during CO₂ adsorption, and comparison with molecular simulations

3.1. Adsorption gravimetry

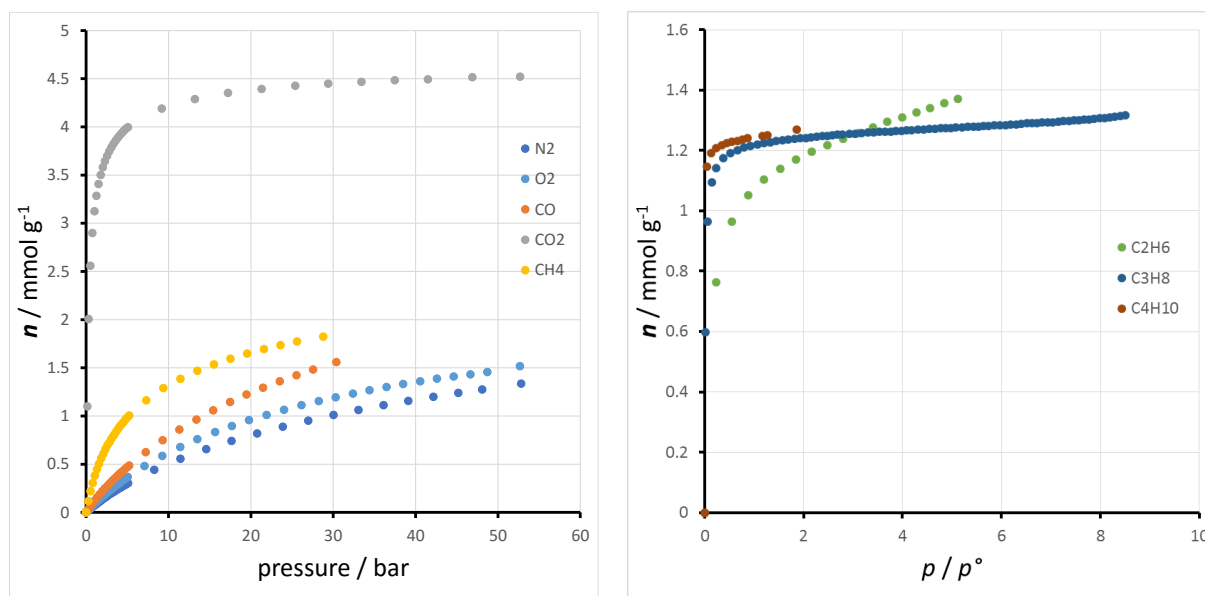


Figure S11. Gravimetric uptakes of a series of gases obtained at 30°C.

To complete the study with CO₂, CH₄ and N₂, the adsorption of other gases have equally been carried out (Figure S11). The isotherms were obtained using an adsorption gravimetric set-up constructed *in house* based on a Rubotherm balance and homemade dosing system. [5] The MIL-91(Ti) (hydrothermal synthesis) sample was outgassed to 150°C, overnight under secondary vacuum.

Several comparisons can be made. There is a slightly higher uptake of oxygen with respect to nitrogen. The adsorption of carbon monoxide is also relatively low and below that of methane. Propane and butane show very similar uptakes which are much lower than CO₂. The adsorption of ethane shows increasing uptake up to the point where the experiment is stopped (5 bars) which suggest that pore filling is not complete.

3.2. Synchrotron PXRD during CO₂ adsorption

In situ synchrotron power diffraction experiments were carried out at the BM01A station at the Swiss-Norwegian Beamlines at the European Synchrotron radiation facility (Grenoble, France). The data were collected on 0.5-mm quartz capillaries filled with sample and attached to a built gas manifold. [6] The sample capillary was placed at 300 mm from a MAR345 image plate detector and an X-ray wavelength of 0.694018 Å was used. The data were integrated using Fit2D program (Dr. A. Hammersley, ESRF) and a calibration measurement of a NIST LaB6 standard sample. The patterns were indexed using the Dicvol software. [7] Le Bail fits were then performed with Fullprof2k software package. [8] The carbon dioxide (Alphagaz, France, 99.9999% purity) was introduced using point by point dosing up to the desirable pressure. Equilibrium was assumed when two successively measured diffraction patterns were identical.

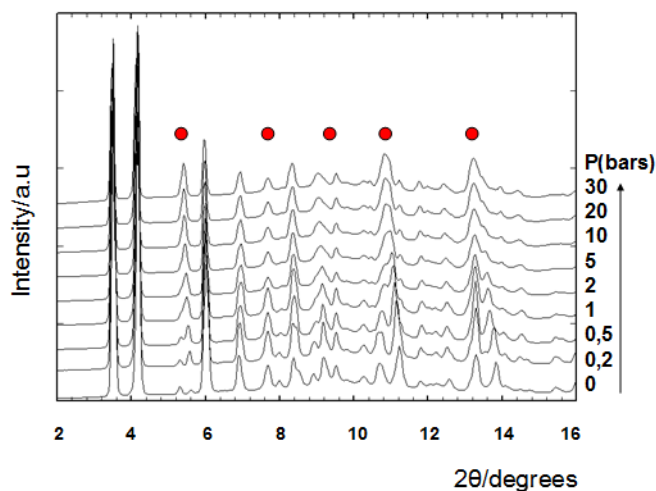


Figure S12. Diffractograms for various CO₂ pressures (303K) measured on MIL-91(Ti) ($\lambda=0.694018\text{\AA}$). The first diffractogram, at $p=0$, corresponds to the dehydrated phase.

The diffraction patterns (Figure S12) show little change in position with loading and no large changes in the patterns is observed. Modeling the unit cell of the empty and filled structure suggest a 1.6% change in unit cell volume.

3.3. Comparison of the adsorption properties between different MOFs

Table S3. Comparison of initial adsorption energies of CO₂, N₂ and CH₄ obtained at 30°C by microcalorimetry with various MOFs. Differences in enthalpies, which are discussed in the main text, are equally given.

| Sample | CO ₂ | CH ₄ | N ₂ | $\Delta[\text{CO}_2\text{-CH}_4]$ | $\Delta[\text{CO}_2\text{-N}_2]$ | reference |
|-----------------------------|-----------------|-----------------|----------------|-----------------------------------|----------------------------------|------------------|
| CAU-13(Al) | 37.3 | 29.7 | 25.2 | 7.6 | 12.1 | [9] |
| CPO-27(Ni) | 38.0 | 20.0 | 22.0 | 18.0 | 16.0 | [10] |
| CuBTC | 29.1 | 20.9 | 15.2 | 8.2 | 13.9 | [11] |
| MIL-100(Fe) | 38.4 | 14.8 | 21.7 | 23.6 | 16.7 | [13] |
| MIL-101(Cr) | 62.8 | 17.0 | 33.6 | 45.8 | 29.3 | [13] |
| MIL-102(Cr) | 47.0 | 29.0 | 44.0 | 18.0 | 3.0 | [14] |
| MIL-125(Ti) | 26.2 | 17.4 | 14.5 | 8.8 | 11.7 | [15] |
| MIL-125(Ti)_NH ₂ | 29.7 | 19.3 | 16.6 | 10.4 | 13.1 | [15] |
| MIL-140A(Zr) | 29.7 | 17.3 | 18.0 | 12.4 | 11.7 | [16] |
| MIL-47(V) | 21.5 | 15.0 | / | 6.5 | / | [17] |
| MIL53(Al)_NH ₂ | 41.5 | 23.0 | 12.0 | 18.5 | 29.5 | [18] |
| MIL-68(Ga) | 28.3 | 24.5 | / | 3.8 | / | [19] |
| MIL-91(Al) | 38.5 | 24.2 | / | 14.3 | / | [20] |
| MIL-91(Ti) HT | 47.1 | 23.8 | 19.5 | 23.3 | 27.6 | This work |
| MIL-91(Ti) RF | 40.4 | 23.5 | 20.1 | 16.9 | 23.5 | This work |
| NaX | 49.0 | 19.4 | 18.0 | 29.6 | 31.0 | [21] |
| ScBDC | 31.8 | 16.7 | / | 15.1 | / | [22] |
| ScBDC_NH ₂ | 45.3 | 17.3 | / | 28.0 | / | [23] |
| STA-12(Ni) | 33.7 | 13.6 | / | 20.2 | / | [24] |
| Takeda 5A | 33.8 | 24.0 | 16.4 | 9.8 | 17.4 | [21] |
| UiO-66(Zr) | 26.4 | 15.9 | 14.8 | 10.5 | 11.7 | [25] |
| UiO-66(Zr)_BTeC | 35.0 | 22.8 | 18.0 | 12.2 | 17.1 | [26] |
| UiO-66(Zr)_NH ₂ | 36.0 | 19.7 | 17.7 | 16.3 | 18.2 | [27] |

Table S4. Comparison of working capacities for CO₂ / N₂ and CO₂ / CH₄ separations at 30°C.

| Sample | WC[CO ₂ /N ₂] / cm ³ .cm ⁻³ (0-1 bar, 303K) | WC[CO ₂ /CH ₄] / cm ³ .cm ⁻³ (1-15 bar, 303K) | Ref |
|-----------------------------|---|---|------------------|
| CAU-13(Al) | 35 | 13.4 | [9] |
| CPO-27(Ni) | 175 | 21.1 | [10] |
| CuBTC | 180 | 14.1 | [11] |
| MIL-100(Fe) | 136.2 | 15.5 | [13] |
| MIL-101(Cr) | 112 | 16.14 | [13] |
| MIL-102(Cr) | 73 | 37.12 | [14] |
| MIL-125(Ti) | 153 | 4.9 | [15] |
| MIL-125(Ti)_NH ₂ | 129 | 9.8 | [15] |
| MIL-140A(Zr) | 69.45 | 4.2 | [16] |
| MIL-47(V) | 162 | / | [17] |
| MIL53(Al)_NH ₂ | 10.1 | 18.8 | [18] |
| MIL-68(Ga) | 75 | 1.6 | [19] |
| MIL-91(Al) | 31.5 | 15.5 | [20] |
| MIL-91(Ti) HT | 50.9 | 43.5 | This work |
| NaX | 70.5 | / | [21] |
| ScBDC | 73.1 | 8.27 | [22] |
| ScBDC_NH ₂ | 31.7 | 5.1 | [23] |
| STA-12(Ni) | 242 | / | [24] |
| Takeda 5A | 110 | 11.25 | [21] |
| UiO-66(Zr) | 175.2 | 7.1 | [25] |
| UiO-66(Zr)_BTeC | 87.06 | 13.68 | [27] |
| UiO-66(Zr)_NH ₂ | 125 | 22.31 | [27] |

Table S5. Comparison of the selectivities for CO₂ / N₂ and CO₂ / CH₄ (1) Calculated in this study.

| Sample | Selectivity CO ₂ / N ₂ (15% CO ₂ , 0-1 bar, 303 K) | Selectivity CO ₂ / CH ₄ (1-50% CO ₂ , 15 bar, 303 K) |
|-----------------------------|--|--|
| CAU-13(Al) | 22 * | 3 * |
| CPO-27(Ni) | 13 * | 7 * |
| CuBTC | 19 * | 7 * |
| MIL-100(Fe) | 47 * | 14 * |
| MIL-101(Cr) | 53 * | 16 * |
| MIL-102(Cr) | 41 * | 12 * |
| MIL-125(Ti) | 12 * | 5 * |
| MIL-125(Ti)_NH ₂ | 18 * | 6 * |
| MIL-140A(Zr) | 10 * | 4 * |
| MIL-47(V) | / | 4 * |
| MIL53(Al)_NH ₂ | 877 * | 7 * |
| MIL-68(Ga) | 12 * | 4 * |
| MIL-69(Al) | 120 * | 4 * |
| MIL-69(Fe) | 6 * | / |
| MIL-91(Al) | 68 * | 57 * |
| MIL-91(Ti) HT | 150 * | 79 * |
| NaX | / | 212 * |
| ScBDC | 40 * | 9 * |
| ScBDC_NH ₂ | 120 * | 17 * |
| STA-12(Ni) | / | 15 * |
| Takeda 5A | 19 * | 4 * |
| UiO-66 (Zr) | 12 * | 6 * |
| UiO-66(Zr)_Br | 30 * | 6 * |
| UiO-66(Zr)_BTeC | 30 * | 9 * |
| UiO-66(Zr)_NH ₂ | 37 * | 11 * |

- * Calculated using IAST

Table S6. Comparison of the selectivities for CO₂ / N₂ and CO₂ / CH₄ (2) Obtained from the open literature

| Name | Mixture | %CO ₂ in mixture | Selectivity | Calculation method | Ref |
|--|----------------------------------|-----------------------------|-------------|--------------------|------|
| MIL-68(Al)_NH ₂ | CO ₂ /CH ₄ | 50 | 45 | GCMC | [19] |
| MIL-125(Ti) | CO ₂ /CH ₄ | 50 | 4.5 | Measurement | [15] |
| MIL-125(Ti)_NH ₂ | CO ₂ /CH ₄ | 50 | 7 | VSM / GCMC | [15] |
| MIL-53(Al) Basolie A100 | CO ₂ /CH ₄ | 50 | 7 | Measurement | [28] |
| MIL-100(Cr) | CO ₂ /CH ₄ | 50 | 6-8 | Measurement | [29] |
| eea-MOF-4 | CO ₂ /CH ₄ | 50 | 4 | IAST | [30] |
| rtl-MOF-2 | CO ₂ /CH ₄ | 50 | 7-8 | IAST | [30] |
| SIFSIX-2Cu-i | CO ₂ /CH ₄ | 50 | 50 | Measurement | [31] |
| MIL-100(V) | CO ₂ /CH ₄ | 50 | 140 | IAST | [32] |
| eea-MOF-4 | CO ₂ /N ₂ | 10 | 18 | IAST | [30] |
| rtl-MOF-2 | CO ₂ /N ₂ | 10 | 38 | IAST | [30] |
| SIFSIX-2Cu-i | CO ₂ /N ₂ | 10 | 72 | Measurement | [31] |
| Eu fcu-MOF | CO ₂ /N ₂ | 10 | 82 | IAST | [33] |
| SIFSIX-3-Cu | CO ₂ /N ₂ | 10 | Infinite | IAST | [34] |
| Zn ₄ (pydc) ₄ (DMF) ₂ ·3DMF | CO ₂ /N ₂ | 15 | 42 | IAST | [35] |
| MOF-508b | CO ₂ /CH ₄ | 50 | 3.5 | Measurement | [36] |
| MIL-53(Al) | CO ₂ /CH ₄ | 50 | 7-8 | Measurement | [37] |
| MIL-53(Cr) | CO ₂ /CH ₄ | 50 | 4-14 | Measurement | [38] |
| Cu-BTC | CO ₂ /CH ₄ | 50 | 6-9 | Measurement | [39] |
| IFP-5 (Imidazolate Framework Postdam) | CO ₂ /CH ₄ | 50 | 7.5 | Measurement | [40] |
| ZIF-176 | CO ₂ /CH ₄ | 50 | 2.5-6.5 | Measurement | [41] |
| UiO-66 (Zr) BTEC | CO ₂ /N ₂ | 15 | 56 | Measurement | [42] |
| Ni/DOBDC | CO ₂ /N ₂ | 15 | 38 | Measurement | [43] |
| USTA-16 | CO ₂ /CH ₄ | 50 | 30 | Measurement | [44] |
| USTA-16 | CO ₂ /N ₂ | 15 | 315 | Measurement | [44] |

4. Mixture adsorption

In order to acquire mixture adsorption equilibrium data, we used a home-made volumetric apparatus as shown in Figure S13.

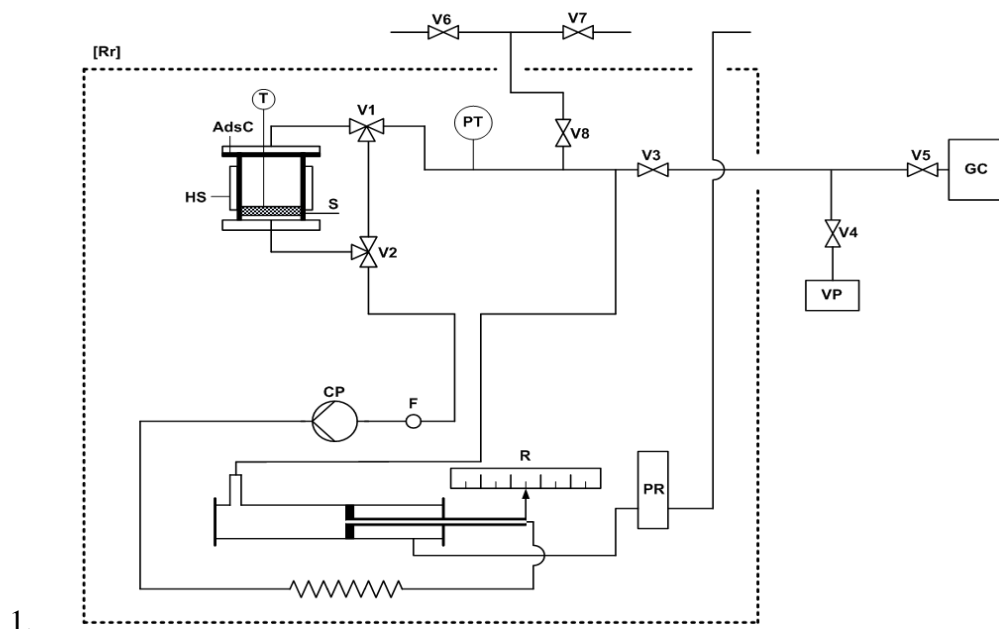


Figure S13. Mixture adsorption volumetric apparatus: (AdsC) adsorption cell; (PT) pressure transmitter; (V1 and V2) three way manual valves; (V3 to V8) manual valves; (T) Pt-100 temperature probe; (F) filter; (HS) in-situ heating system; (VP) vacuum pump; (CP) circulation pump; (R) ruler; (PR) pressure regulator; (GC) gas chromatograph; (Rr) refrigerated room.

The volumetric co-adsorption measurements ^[45, 46] is based on the principle of pure compound manometric apparatus. ^[47-49]

The apparatus allows the measurement of isobaric-isothermal mixture adsorption equilibria in a pressure range from 1 to 10 bar and in a temperature range from 298 K to 353 K. In this apparatus, a cylinder piston provides a variable volume in order to fix the pressure on a set point value during the adsorption. A circulation pump was used to homogenize the mixture and a gas chromatograph coupled with a thermal conductivity detector, provided by Agilent (GC 6850), allowing the determination of the gas mole fraction of each component in the mixture. The pressure transmitter provided by Endress-Hauser (0 – 10 bar Cerabar PMP 731) with an uncertainty of 0.1% of the full scale. The adsorbent was outgassed by maintaining it under primary vacuum at ambient temperature for one hour and then by heating the

adsorption cell up to 453 K for 8 hours. After that, the gas mixture was introduced in the installation without going through the adsorption cell. When both equilibrium and homogenization were reached (checked by constant values of both pressure and composition obtained using a chromatography device), the gas composition was determined after at least six chromatographic analyses and the pressure and temperature values were recorded. With these measurements and the installation volume, we can determine the adsorption amounts of the two components in each mixture using a mixture equation of state.^[50]

In the second phase, the adsorption cell was controlled to be accessible via two three-way valves. During the adsorption, the pressure was maintained on a set point value by adapting the installation volume using the cylinder piston. When the equilibrium was reached, the pressure, temperature and volume of the system were recorded and the gas composition was determined by at least six chromatographic analyses. Knowing the total installation volume, the amount of each component in the gas phase after adsorption can be calculated using the mixture equation of state adopted by Myers and Prausnitz.^[51]

The adsorbed amounts were determined by the differences between the number of moles in the gas phase before and after adsorption. Finally, the adsorbent was outgassed to repeat the above procedures with a new composition of the initial mixture.

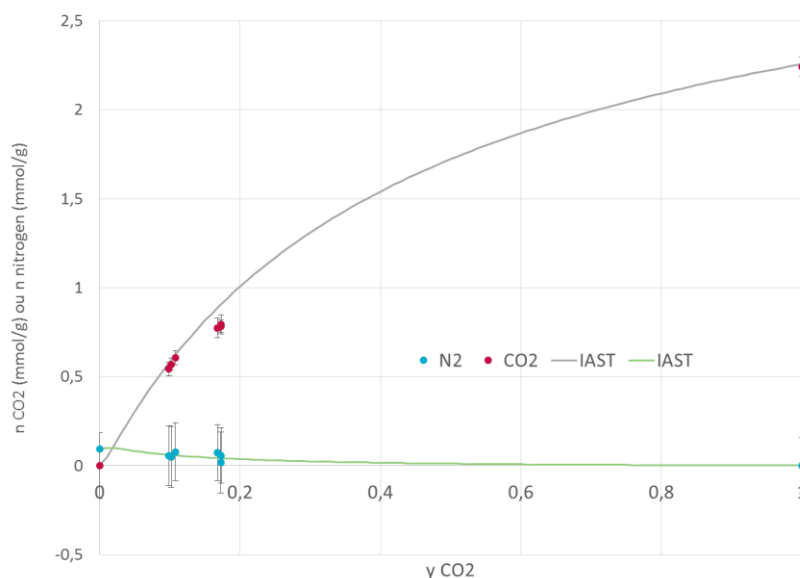


Figure S14 : Mixture adsorption results obtained with approximately 10% and 17% CO_2 in N_2 at a total pressure of 1 bar and at 30°C. Experiments at each concentration were repeated. The straight line fit corresponds to the IAST prediction from single gas data.

Table S7 : CO₂ / N₂ selectivities measured and calculated at 30°C

| Total pressure | % CO₂ | Measured selectivity | Average measured selectivity | Selectivity calculated by IAST |
|-----------------------|-------------------------|-----------------------------|-------------------------------------|---------------------------------------|
| 1 bar | 0,108 | 65 | | |
| | 0,099 | 89 | 86 | 87 |
| | 0,102 | 106 | | |
| | 0,173 | 67 | | |
| | 0,168 | 53 | 60 | 99 |
| 3 bars | 0,103 | 89 | | |
| | 0,117 | 61 | 73 | 130 |
| | 0,118 | 69 | | |
| | 0,176 | 60 | | |
| | 0,169 | 49 | 51 | 153 |
| | 0,168 | 45 | | |

Table S8 : CO₂ / CH₄ selectivities obtained at 30°C

| Total pressure | % CO₂ | Measured selectivity | Selectivity calculated by IAST |
|-----------------------|-------------------------|-----------------------------|---------------------------------------|
| 1 bar | 50 | 18 | 31 |
| 5 bars | 50 | 15 | 74 |
| 13 bars | 50 | 13 | |

5. Quasi-Elastic neutron scattering measurements

The QENS experiments were carried out with the time-of-flight spectrometer IN6, at the Institut Laue-Langevin, Grenoble, France. The incident neutron energy was set to 5.12 Å, corresponding to an incident energy of 3.12 meV. Scattered neutrons were analyzed as a function of angle and flight time. Groupings of detectors were made to avoid the Bragg peaks of MIL-91 and to obtain satisfactory counting statistics, the wave-vector transfer, Q , ranging from 0.29 to 1.19 Å⁻¹. The elastic energy resolution could be fitted by a Gaussian function, with a half-width at half-maximum varying from 39 μeV at small Q to 46 μeV at large Q .

The framework of MIL-91 was deuterated, in order to measure the signal from weak scatterers such as CO₂ and N₂. The MIL-91 sample was activated by pumping at 423 K. The powder was transferred inside a glovebox into a slab-shaped aluminum container, which was connected to a gas inlet system allowing in situ adsorption. After recording the scattering of the empty MOF, a loading of 0.7 N₂ per unit cell were measured at 220 K. After these measurements, N₂ was evacuated by pumping at 370 K. A CO₂ loading of 1.2 molecules per unit cell were then studied at 300 K.

6. Molecular simulations .

6.1. Computational Methods

6.1.1. Microscopic models for the host framework.

The experimental dry (hereafter MIL-91(Ti)_Dry)^[51] and CO₂ loaded MIL-91(Ti) (hereafter MIL-91(Ti)_CO₂) crystal structures were preliminary saturated by the missing hydrogen atoms using Materials Studio software package (Figure S15). While the hydrogen atoms were added to the carbon atoms of the organic linkers, the mobile proton in the environment of the piperazine bis methylphosphonate groups, labeled as PO...H...N, was arbitrary placed on the O atoms. The MIL-91(Ti)_dry crystal structure was then geometry optimized at the Density Functional Theory (DFT) level using the CP2K package^[53-55]. These calculations included only the relaxation of the positions of the atoms of the framework while the unit cell parameters were fixed at the values previously determined by PXRD analysis (Table S9)^[52]. The PBE^[56] functional was combined with the use of Gaussian basis

set and pseudopotential. For Carbon, Oxygen, Nitrogen, Phosphorous and Hydrogen, a triple zeta (TZVP-MOLOPT) basis set was considered, while a double zeta (DZVP-MOLOPT) was applied for Titanium. [57] The pseudopotentials used for all of the atoms were those derived by Goedecker, Teter and Hutter. [57] The van der Waals effects interactions were taken into account via the use of semi-empirical dispersion corrections as implemented in the DFT-D3 method. [59]

The crystal structure of the CO₂ loaded MIL-91(Ti) material experimentally refined at 30 bar and 235 K was first loaded with 4.5 mmol g⁻¹ of CO₂ (i.e. the saturation capacity obtained experimentally at 303 K and 30 bar) and then fully relaxed (both atomic positions of the framework and the CO₂ molecules, and cell parameters) at the DFT-level keeping the same functional and basis set used for the MIL-91(Ti)_Dry structure. The optimized unit cell parameters for this structure labelled as MIL-91(Ti)_CO₂ are reported in Table S9.

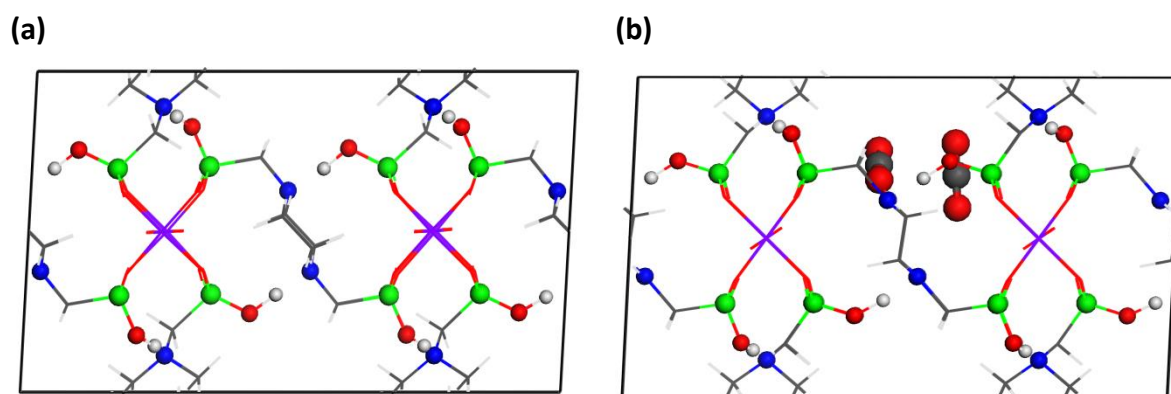


Figure S15. The simulation box considered for the DFT calculations (1×2×1 unit cells) viewed along *b* direction for MIL-91(Ti)_Dry (a) and MIL-91(Ti)_CO₂ (b), where identified interaction sites are represented by ball, and the rest of the atoms are in line representation. (Gray, carbon; white, hydrogen; blue, nitrogen; green, phosphorous; red, oxygen; violet, titanium).

Table S1_9. Comparison of the experimental and simulated unit cell parameters/symmetry obtained for the dry and the CO₂ loaded MIL-91(Ti) structures.

| | Space Group | a (Å) | b (Å) | c (Å) | β(°) | v (Å ³) |
|----------------------------|-------------|---------|--------|---------|--------|---------------------|
| MIL-91(Ti)_CO ₂ | | | | | | |
| Simulation | C2/m | 18.7250 | 7.1760 | 11.8960 | 99.607 | 1576.05 |
| Experimental | C2/m | 19.4146 | 7.0716 | 11.4834 | 92.779 | 1574.73 |

MIL-91(Ti)_Dry

Experimental C2/m 19.0599 7.0499 11.3049 93.100 1516.86

The Mulliken ^[60] partial charges for all atoms of the MOF framework were further obtained by performing a single point energy calculation on the MIL-91(Ti)_Dry structure using Dmol³ (see Tables S10, Figure S17). These calculations were also based on the PBE functional and the double numerical basis set containing polarization functions (DNP). ^[61]

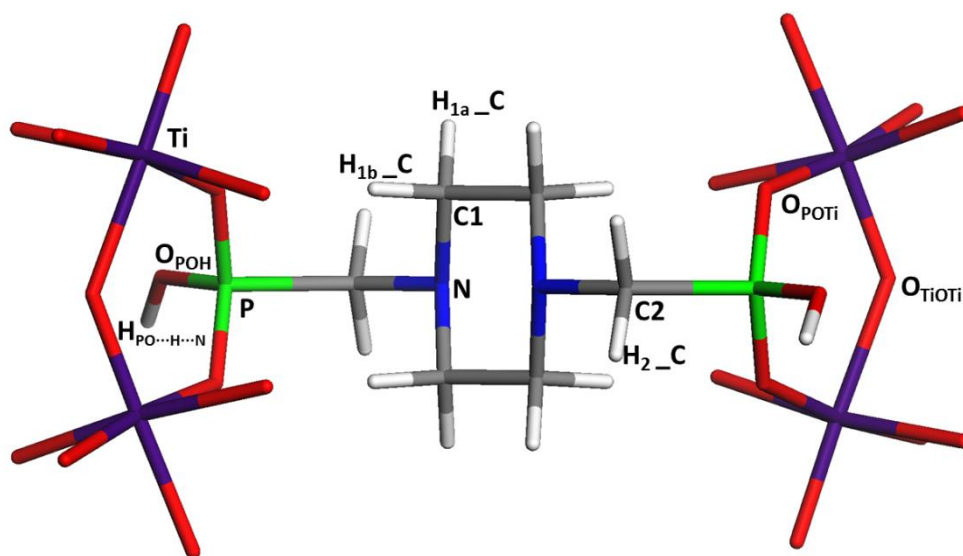


Figure S16. Labels of the atoms for the organic and the inorganic parts of the MOF structure. The color code is the same as the one reported in Figure S15.

Table S10. Mulliken partial charges for the atoms in MIL-91(Ti)

| Atom types | C1 | C2 | H _{1a_C} | H _{1b_C} | H _{2_C} | H _{PO...H...N} | N | O _{TiOTi} | O _{POTi} | O _{POH} | P | Ti |
|------------|--------|--------|-------------------|-------------------|------------------|-------------------------|--------|--------------------|-------------------|------------------|-------|-------|
| Charge | -0.115 | -0.371 | 0.246 | 0.154 | 0.159 | 0.405 | -0.432 | -0.734 | -0.748 | -0.794 | 1.465 | 1.404 |

(e)

6.1.2. Force fields

The interaction between the MIL-91(Ti) framework and the guest species (CO₂, CH₄ and N₂) was modelled using the sum of a 12-6 Lennard-Jones (LJ) contribution and a Coulombic term. The Universal force field (UFF) was adopted to describe the LJ parameters for the atoms of the MOF framework (see Figure S16 and Table S11). ^[62] CO₂ was represented using the 3-

sites charged EPM2 model ^[63] while CH₄ and N₂ were treated by the uncharged united atom (UA) models.^[64]

Table S11. LJ potential parameters for the framework atoms in the MIL-91(Ti) according to the notation introduced in Figure S15. The attractive van der Waals force exerted by the Ti atom is not considered as this atom is screened by its oxygen environment. The same kind of interaction is neglected for the mobile proton in the environment of the piperazine bis methylphosphonate groups to be consistent with our previous studies on MIL-91(Al) ^[20]

| Atom type | σ (Å) | ϵ/k_B (K) |
|-------------------------------|--------------|--------------------|
| C1 | 3.431 | 52.838 |
| C2 | 3.431 | 52.838 |
| H_{1a}_C | 2.571 | 22.141 |
| H_{1b}_C | 2.571 | 22.141 |
| H₂_C | 2.571 | 22.141 |
| H_{PO...H...N} | 2.571 | 0.000* |
| N | 3.261 | 34.721 |
| O_{OTiP} | 3.118 | 30.193 |
| O_{OTiO} | 3.118 | 30.193 |
| O_{PO} | 3.118 | 30.193 |
| P | 3.695 | 153.482 |
| Ti | 2.829 | 0.000* |

6.2. GCMC Simulations

Grand Canonical Monte Carlo (GCMC) simulations were carried out at 303 K for MIL-91(Ti)_CO₂ in order to predict the single component adsorption of CO₂ and their binary CO₂/N₂ and CO₂/CH₄ mixtures while the crystal structure for MIL-91(Ti)_Dry has been selected for the investigation of the single components CH₄ and N₂. These calculations were performed using the Complex Adsorption and Diffusion Simulation Suite (CADSS) code. ^[65] The simulation box was made of 24 (2×4×3) unit cells of MIL-91(Ti)_CO₂. Short-range dispersion forces were truncated at a cutoff radius of 12 Å while the interactions between unlike force field centers *a* and *b* were treated by means of the Lorentz-Berthelot

combination rules; $\varepsilon_{ab} = \sqrt{\varepsilon_a \varepsilon_b}$, $\sigma_{ab} = (\sigma_a + \sigma_b)/2$, where ε_a and σ_a are the LJ parameters for the species a . The long-range electrostatic interactions were handled using the Ewald summation technique.

The fugacities for each adsorbed species at a given thermodynamic condition were computed with the Peng-Robinson equation of state (EoS).^[66] For each state point, 2×10^8 Monte Carlo steps have been used for both equilibration and production runs. Three types of trials were considered for the molecules: (i) translation or rotation, (ii) creation/deletion and (iii) exchange of molecular identity. The adsorption enthalpy at low coverage (Δh) for each gas was calculated through configurational-bias Monte Carlo simulations performed in the NVT ensemble using the revised Widom's test particle insertion method.^[67] Additionally, in order to gain insight into the configurational distribution of the adsorbed species in MIL-91(Ti), some additional data were calculated at different pressure including the radial distribution functions (RDF) between the guests and the host.

6.3. Computational predictions

The cell dimension of the DFT-simulated CO₂ loaded MIL-91(Ti) structure ($V = 1576.05 \text{ \AA}^3$) is in very good agreement with the one ($V = 1574.73 \text{ \AA}^3$) determined from the *in situ* X-ray diffraction (Table S9). It can be seen from Figure S15 that the piperazine linkers are reoriented upon CO₂ adsorption resulting into a more tight packing of the adsorbate molecules. These DFT simulations also reveal that the CO₂ molecules are preferentially located in the vicinity of the phosphonate and piperazine linker (i.e. zwitterionic site of this solid), consistent with the experimental observation. The CO₂ molecule aligned in such a way that carbon atom of C=O group (C_{CO_2}) interact with O atom present in the environment of the PO group and the N atom ($PO \cdots H \cdots N$), giving a $C_{CO_2} - O_{PO \cdots H \cdots N}$ distance of 2.68 \AA , similar to the one obtained experimentally (see Figure S17). Such a spatial distribution leads the oxygen atoms of CO₂ (O_{CO_2}) to interact with the H atom in the $PO \cdots H \cdots N$ environment, ($H_{PO \cdots H \cdots N}$) with a distance of 3.42 \AA .

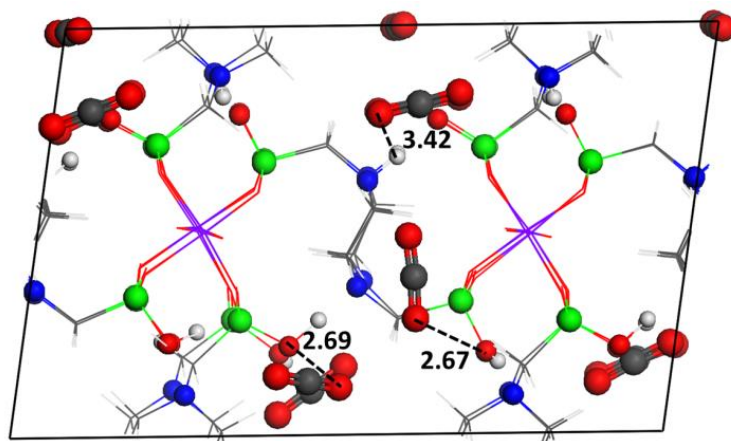


Figure S17. The CO₂ loaded MIL-91(Ti) crystal structure (MIL-91(Ti)_CO₂) determined by DFT geometry optimization. The color code is the same as the one reported in Figure S1.

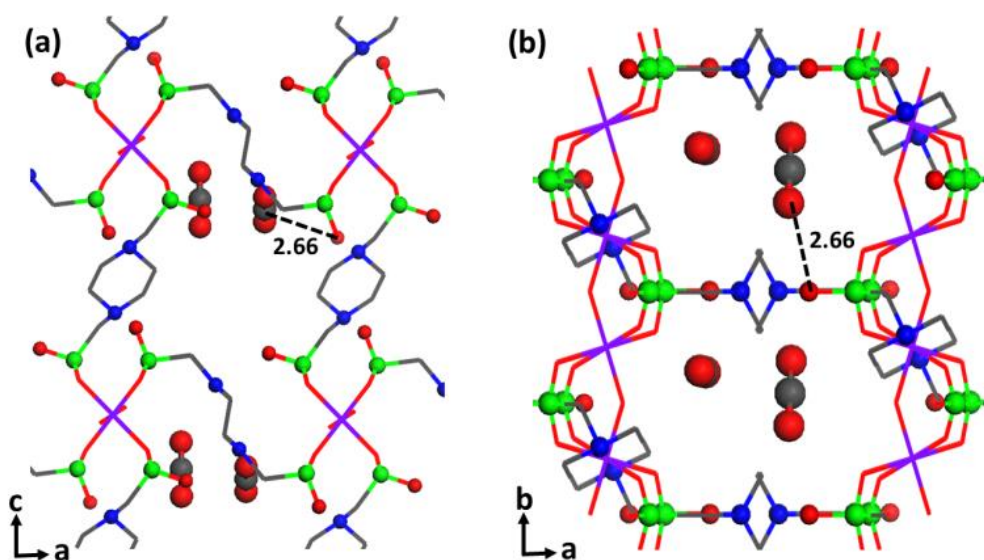


Figure S18. Illustration of the preferential ordered arrangement of CO₂ experimentally obtained from the refinement of the XRPD patterns. Views along *b* (a) and *c* (b) vector directions. The color code is the same as the one reported in Figure S15.

This validated MIL-91(Ti)_CO₂ model was further used to predict the single component adsorption isotherms at 303 K by means of GCMC simulations. We have obtained a good agreement between the simulated and the experimental adsorption isotherms at the entire pressure range [0-35 bar]. Analysis of the adsorption mechanism evidences that the simulated CO₂ distribution matches well with the one obtained by DFT calculations. The radial distribution function (RDF) analysis (Figure S19) for CO₂ in MIL-91(Ti)_CO₂ shows that

the mean distances between $C_{CO_2} - O_{PO\cdots H\cdots N}$ and $O_{CO_2} - H_{PO\cdots H\cdots N}$ are 2.71 and 3.48 Å, respectively. As expected, the preferential interactions occur between CO_2 and the zwitterionic sites of the solid, where H atom present in the environment of the PO group and the N atom ($PO\cdots H\cdots N$). Such a geometry (Figure S20) is consistent with has been already reported for the Al version, i.e. MIL-91(Al), [20] with the presence of a dual acid-base interaction: the O atom of CO_2 interacting with an acid site, the C atom playing the role of an electron acceptor centre towards the oxygen basic site. [67, 68]

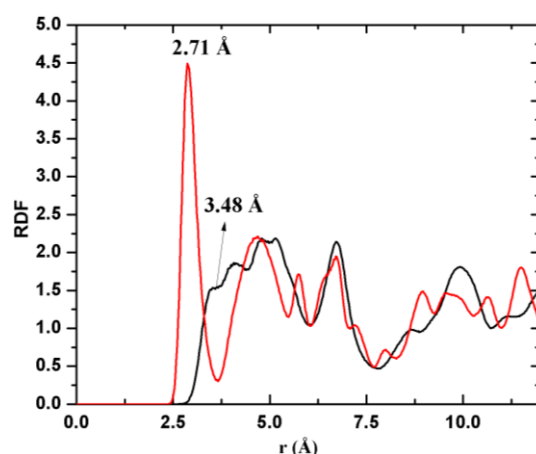


Figure S19: Radial Distribution Functions (RDF) for the pairs $C_{CO_2} - O_{PO\cdots H\cdots N}$ (red) and $H_{PO\cdots H\cdots N} - O_{CO_2}$ (black) extracted from the GCMC simulations at 303 K for MIL-91(Ti) $_CO_2$ with two CO_2 molecule per unit cell.

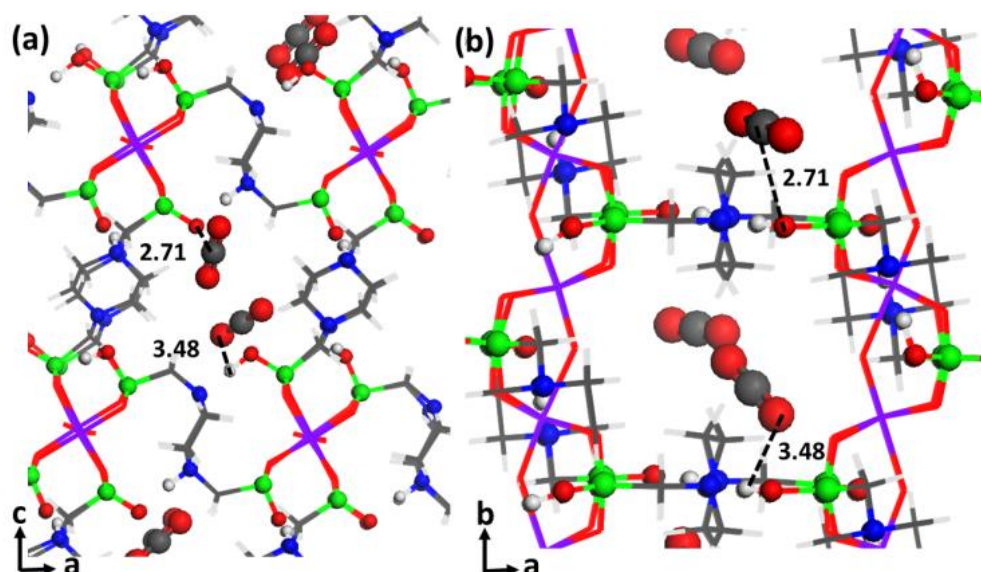


Figure S20. GCMC simulated arrangements of CO_2 molecules obtained using MIL-91(Ti) $_CO_2$ models at 303 K viewed along b (a) and c (b) vector. The snapshots were taken from the

simulations performed for 2 CO₂ molecules per unit cell adsorbed framework. The color code is the same as the one reported in Figure S15.

This preferential arrangement of CO₂ within the pores leads to a relatively high simulated adsorption enthalpy at low coverage (-44 kJ/mol) which is validated by microcalorimetry measurements (Figure S21).

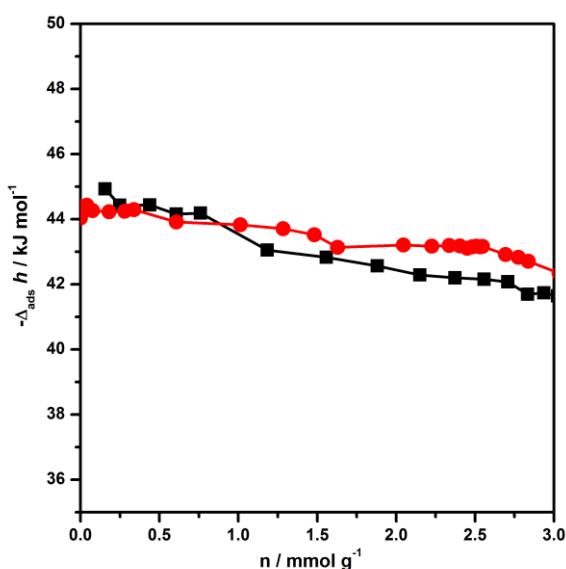


Figure S21. Experimental (black squares) and simulated (red circles) enthalpy obtained by GCMC simulation with CO₂ on MIL-91(Ti) at 303 K.

The binary mixture study was further carried out for CO₂/N₂ (gas phase composition: 0.05/0.95; 0.10/0.90 and 0.15/0.85) and CO₂/CH₄ (gas phase composition: 05/0.5) by means of GCMC simulations performed at 303 K and 313 K. Analysis of the co-adsorption mechanism for both mixtures evidenced that CO₂ molecules are mainly distributed in the same region of the pores than in the single components, i.e. in the vicinity of the PO···H···N sites, mean distances between C_{CO2} and O_{PO···H···N} for CO₂/N₂ and CO₂/CH₄ systems at 2.69 and 2.72 Å, respectively. Similarly, the distances between O_{CO2} and H_{PO···H···N} are 3.49 Å and 3.46 Å for co-adsorption of CO₂ in the presence of N₂ and CH₄, respectively (Figure S22). Furthermore, both N₂ and CH₄ in are distributed in the centre of the pore with very characteristic host/guest distances over 3.2 Å (N₂ - PO···H···N : Figure S23; CH₄ - PO···H···N : Figure S24). Therefore, the CO₂ molecules are interacting strongly with the PO···H···N sites, while the two other gases, N₂ and CH₄, are away from these adsorption sites and fit at the centre of pore.

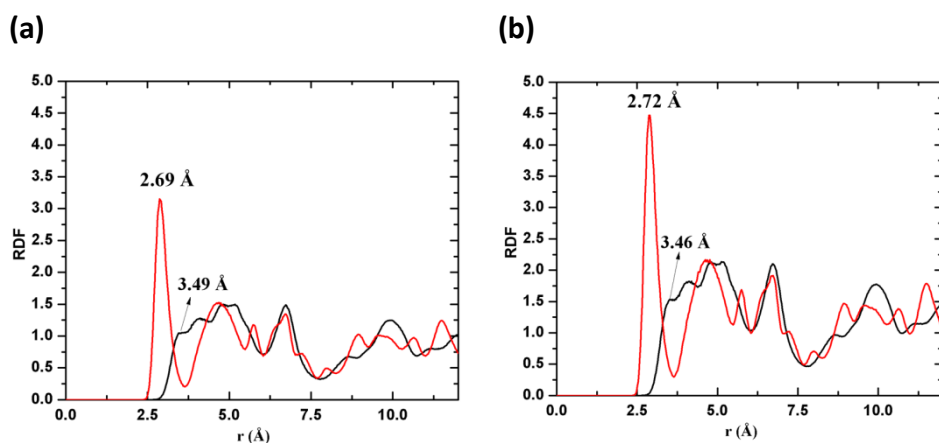


Figure S22: RDF for the pairs $\text{CO}_2 - \text{O}_{\text{PO}\cdots\text{H}\cdots\text{N}}$ (red) and $\text{H}_{\text{PO}\cdots\text{H}\cdots\text{N}} - \text{O}_{\text{CO}_2}$ (black) extracted from the GCMC simulations at 303 K for the mixture with N_2 (a) and CH_4 (b).

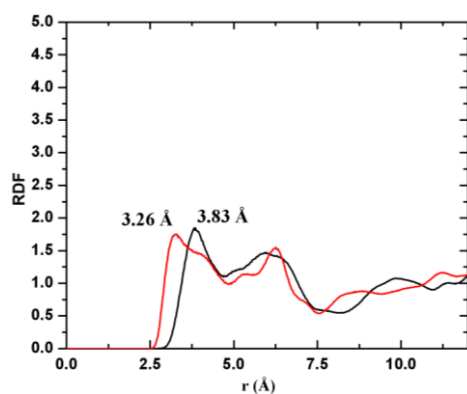


Figure S23: RDF for the pairs $\text{N}_2 - \text{O}_{\text{PO}\cdots\text{H}\cdots\text{N}}$ (red) and $\text{H}_{\text{PO}\cdots\text{H}\cdots\text{N}} - \text{N}_2$ (black) extracted from the GCMC simulations at 303 K for the mixture with CO_2 .

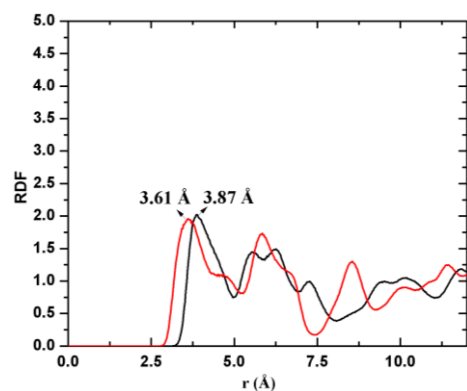


Figure S24: RDF for the pairs $\text{CH}_4 - \text{O}_{\text{PO}\cdots\text{H}\cdots\text{N}}$ (red) and $\text{H}_{\text{PO}\cdots\text{H}\cdots\text{N}} - \text{CH}_4$ (black) extracted from the GCMC simulations at 303 K for the mixture with CO_2 .

The separation performances of MIL-91(Ti) for the two mixtures of interest, i.e. CO_2/N_2 and CO_2/CH_4 , were predicted as a function of the pressure. These data are reported in Figure S25

and Figure S26. The simulated selectivities obtained at 1 bar and 303 K for both gas mixtures is very similar to the experimental results, i.e. $S(\text{CO}_2/\text{N}_2) = 122.0, 122.0,$ and 118.5 for molar concentrations $\text{CO}_2/\text{N}_2 = 0.05/0.95, 0.10/0.90$ and $0.15/0.85$, respectively, and $S(\text{CO}_2/\text{CH}_4) = 40.9$ at molar concentration of $\text{CO}_2/\text{CH}_4 = 0.5/0.5$.

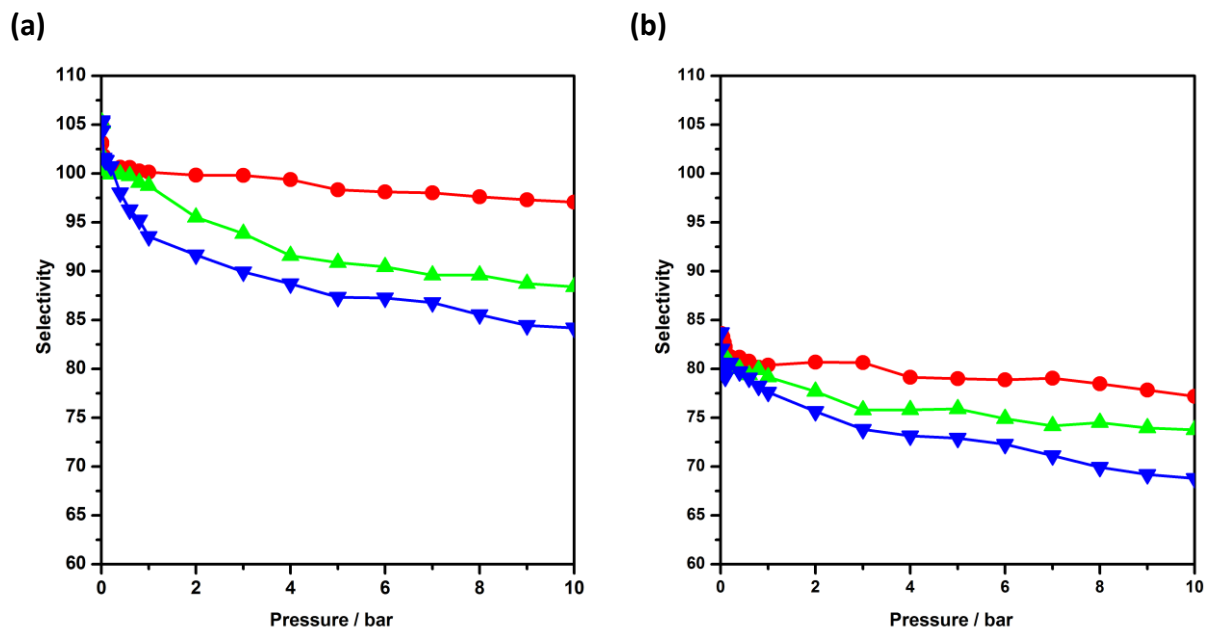


Figure S25. Simulated CO_2/N_2 selectivity at 303 K (a) and 313 K (b) for a molar composition of the gas phase: 0.05/0.95 (CO_2/N_2 , red circles), 0.10/0.90 (CO_2/N_2 , blue up triangles) and 0.15/0.85 (CO_2/N_2 , blue down triangles).

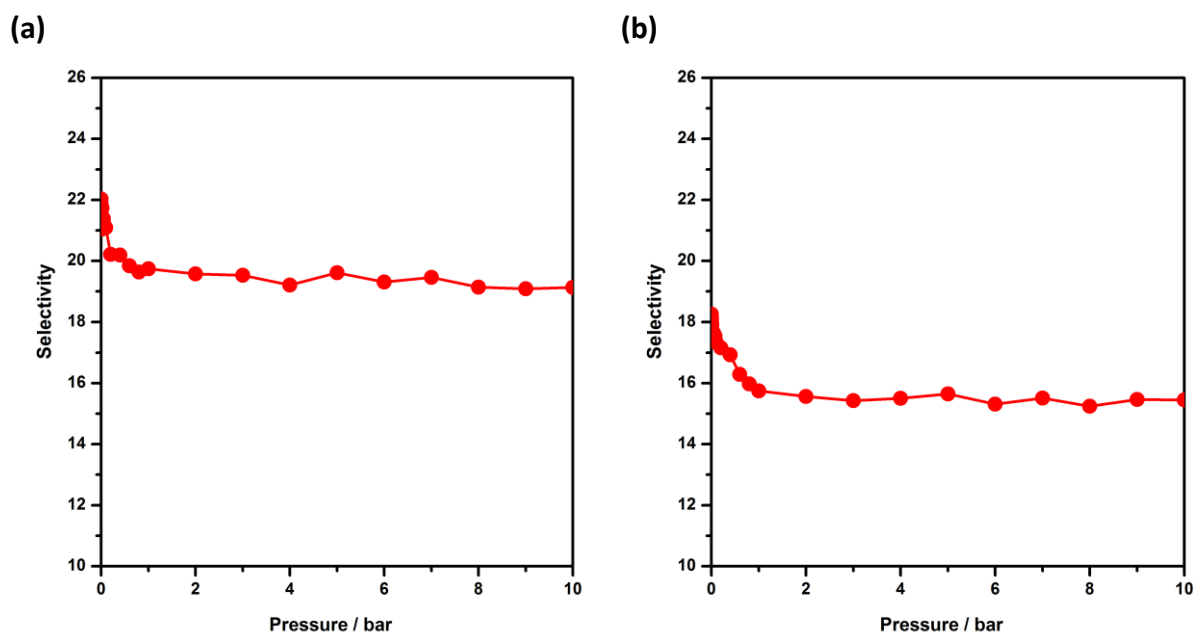


Figure S26. Simulated CO_2/CH_4 Selectivity at 303 K (a) and 313 K (b) for an equimolar composition of the gas phase.

References

- [1] K. Moedritzer and R.R. Irani, *J. Org. Chem.*, **1966**, 31, 1603-1607.
- [2] 10.1515/pac-2014-1117 (2015) (Physisorption of gases, with special reference to the evaluation of surface area and pore size distribution (IUPAC Technical Report))
- [3] J. Rouquerol, F. Rouquerol, P. Llewellyn, G. Maurin, K.S.W. Sing, *Adsorption by Powders and Porous Solids*, 2nd Edition, Academic Press, Oxford, **2014**, 646 pages. ISBN-13: 978-0080970356.
- [4] P.L. Llewellyn, G. Maurin, *C. R. Chim.*, **2005**, 8, 283.
- [5] A. Ghoufi, L. Gaberova, J. Rouquerol, D. Vincent, P. L. Llewellyn, G. Maurin, *Micro. Meso. Mater.*, **2009**, 119(1-3), 117-128.
- [6] P. L. Llewellyn, P. Horcajada, G. Maurin, T. Devic, N. Rosenbach, S. Bourrelly, C. Serre, D. Vincent, S. Loera-Serna, Y. Filinchuk, G. Férey, *J. Amer. Chem. Soc.*, **2009**, 131(36), 13002-13008.
- [7] A. Boultif, D. Löüer, *J. Appl. Crystallogr.*, **1991**, 24, 987-993.
- [8] J. Rodriguez-Carvajal, in *Collected Abstracts of Powder Diffraction Meeting*; Toulouse, France, **1990**; 127-128.
- [9] F. Niekief, J. Lannoeye, H. Reinsch, A. S. Munn, A. Heerwig, I. Zizak, S. Kaskel, R. I. Walton, D. de Vos, P. Llewellyn, A. Lieb, G. Maurin, N. Stock, *Inorg. Chem.*, **2014**, 53(9), 4610-4620.
- [10] W. L. Queen, M. R. Hudson, E. D. Bloch, J. A. Mason, M. I. Gonzalez, J. S. Lee, D. Gygi, J. D. Howe, K. Lee, T. A. Darwish, M. James, V. K. Peterson, S. J. Teat, B. Smit, J. B. Neaton, J. R. Long, C. M. Brown, *Chem. Sci.*, **2014**, 5, 4569.
- [11] L. Grajciar, A. D. Wiersum, P. L. Llewellyn, J.-S. Chang, P. Nachtigall, *J. Phys. Chem. C*, **2011**, 115(36), 17925-17933.
- [12] J. W. Yoon, Y. K. Seo, Y. K. Hwang, J.-S. Chang, H. Leclerc, S. Wuttke, P. Bazin, A. Vimont, M. Daturi, E. Bloch, P. L. Llewellyn, C. Serre, P. Horcajada, J. M. Greneche, A. E. Rodrigues, G. Férey, *Angew. Chem. Int. Ed.*, **2010**, 49(34), 5949-5952.

- [13] P. L. Llewellyn, S. Bourrelly, C. Serre, A. Vimont, M. Daturi, L. Hamon, G. De Weireld, J.-S. Chang, D.-Y. Hong, Y. K. Hwang, S. H. Jung, G. Férey, G., *Langmuir*, **2008**, 24(14), 7245-7250.
- [14] D. Damasceno-Borges, M. Prakash, N.A. Ramsahye, P.L. Llewellyn, S. Surblé, P. Horcajada, C. Serre, G. Maurin, *Mol. Sim.*, **2015**, 41(16-17), 1357-1370.
- [15] S. Vaesen, V. Guillerm, Q. Y. Yang, A. D. Wiersum, B. Marszalek, B. Gil, A. Vimont, M. Daturi, T. Devic, P. L. Llewellyn, C. Serre, G. Maurin, G. De Weireld, *Chem. Comm.*, **2013**, 49(86), 10082-10084.
- [16] G. D. Pirngruber, L. Hamon, S. Bourrelly, P. L. Llewellyn, E. Lenoir, V. Guillerm, C. Serre, T., *ChemSusChem*, **2012**, 5(4), 762-776.
- [17] P. L. Llewellyn, S. Bourrelly, C. Vagner, N. Heymans, H. Leclerc, A. Ghoufi, P. Bazin, A. Vimont, M. Daturi, T. Devic, C. Serre, G. Weireld, G. Maurin, *J. Phys. Chem. C*, **2013**, 117(2), 962-970.
- [18] S. Couck, J. F. M. Denayer, G. V. Baron, T. Remy, J. Gascon, F. Kapteijn, *J. Amer. Chem. Soc.*, **2009**, 131(18), 6326-6327.
- [19] Q. Yang, S. Vaesen, M. Vishnuvarthan, F. Ragon, C. Serre, A. Vimont, M. Daturi, G. De Weireld, G. Maurin, *J. Mater. Chem.*, **2012**, 22(20), 10210-10220
- [20] P. L. Llewellyn, M. Garcia-Rates, L. Gaberova, S. R. Miller, T. Devic, J. C. Lavalley, S. Bourrelly, E. Bloch, Y. Filinchuk, P. A. Wright, C. Serre, A. Vimont, G. Maurin, *J. Phys. Chem. C*, **2015**, 119, 4208-4216.
- [21] A. D. Wiersum, J.-S. Chang, C. Serre, P. L. Llewellyn, *Langmuir*, **2013**, 29(10), 3301-3309.
- [22] S. R. Miller, P. A. Wright, T. Devic, C. Serre, G. Férey, P. L. Llewellyn, R. Denoyel, L. Gaberova, Y. Filinchuk, *Langmuir*, **2009**, 25(6), 3618-3626.
- [23] R. S. Pillai, V. Benoit, A. Orsi, P. L. Llewellyn, P. A. Wright, G. Maurin, *J. Phys. Chem. C*, **2015**, 119 (41), 23592-23598.
- [24] S. R. Miller, G. M. Pearce, P. A. Wright, F. Bonino, S. Chavan, S. Bordiga, I. Margiolaki, N. Guillou, G. Férey, S. Bourrelly, P. L. Llewellyn, *J. Amer. Chem. Soc.*, **2008**, 130(47), 15967-15981.

- [25] Q. Yang, A. D. Wiersum, H. Jobic, V. Guillerm, C. Serre, P. L. Llewellyn, G. Maurin, *J. Phys. Chem. C*, **2011**, 115(28), 13768-13774.
- [26] F. Ragon, B. Campo, Q. Yang, C. Martineau, A. D. Wiersum, A. Lago, V. Guillerm, C. Hemsley, J. F. Eubank, M. Vishnuvarthan, F. Taulelle, P. Horcajada, A. Vimont, P. L. Llewellyn, M. Daturi, S. Devautour-Vinot, G. Maurin, C. Serre, T. Devic, G. Clet, *J. Mater. Chem. C*, **2015**, 3(7), 3294-3309.
- [27] Q. Yang, A. D. Wiersum, P. L. Llewellyn, V. Guillerm, C. Serre, G. Maurin, *Chem. Comm.*, **2011**, 47(34), 9603-9605.
- [28] N. Heymans, S. Vaesen, G. De Weireld, *Micro. Meso. Mat.*, **2012**, 154, 93–99.
- [29] L. Hamon, N. Heymans, P. L. Llewellyn, V. Guillerm, A. Ghoufi, S. Vaesen, G. Maurin, C. Serre, G. De Weireld, G. D. Pirngruber, *Dalton Trans.*, **2012**, 41, 4052.
- [30] Z. Chen, K. Adil, L. J. Weseliński, Y. Belmabkhouta, M. Eddaoudi, *J. Mater. Chem. A*, **2015**, 3, 6276-6281.
- [31] P. Nugent, Y. Belmabkhout, S. D. Burd, A. J. Cairns, R. Luebke, K. Forrest, T. Pham, S. Ma, B. Space, L. Wojtas, M. Eddaoudi, M.J. Zaworotko, *Nature*, **2013**, 495, 80–84.
- [32] J. Yang, Y. Wang, L. Li, Z. Zhang, J. Li, *J. Coll. Interf. Sci.*, **2015**, 456, 197–205.
- [33] D.-X. Xue, Y. Belmabkhout, O. Shekhah, H. Jiang, K. Adil, A. J. Cairns, M. Eddaoudi, *J. Amer. Chem. Soc.*, **2015**, 137, 5034-5040.
- [34] O. Shekhah, Y. Belmabkhout, Z. Chen, V. Guillerm, A. Cairns, K. Adil, M. Eddaoudi, *Nat. Comms.*, **2014**, 5, 4228.
- [35] S. R. Ahrenholtz, C. Landaverde-Alvarado, M. Whiting, S. Lin, C. Slebodnick, E. Marand, A. J. Morris, *Inorg. Chem.*, **2015**, 54(9), 4328-4336.
- [36] P. S. Bárcia, L. Bastin, E. J. Hurtado, J. A. C. Silva, A. E. Rodrigues, B. Chen, *Sep. Sci. Tech.*, **2008**, 43, 3494-3521
- [37] V. Finsy, L. Ma, L. Alaerts, D.E. De Vos, G.V. Baron, J.F.M. Denayer, *Micro. Meso. Mater.*, **2009**, 120, 221–227

- [38] L. Hamon, P. L. Llewellyn, T. Devic, A. Ghoufi, G. Clet, V. Guillerm, G. D. Pirngruber, G. Maurin, C. Serre, G. Driver, W. van Beek, E. Jolimaître, A. Vimont, M. Daturi, G. Férey, *J. Amer. Chem. Soc.*, **2009**, 131, 17490–17499
- [39] Lomig Hamon, Elsa Jolimaître, and Gerhard D. Pirngruber, *Ind. Eng. Chem. Res.*, **2010**, 49(16), 7497–7503
- [40] F. Debatin, J. Möllmer, S. S. Mondal, K. Behrens, A. Möller, R. Staudt, A. Thomas, H.-J. Holdt, *J. Mater. Chem.*, **2012**, 22, 10221
- [41] D. Peralta, G. Chaplais, A. Simon-Masseron, K. Barthelet, G. D. Pirngruber, *Micro. Meso. Mater.*, **2012**, 153, 1–7.
- [42] Q. Yang, S. Vaesen, F. Ragon, A. D. Wiersum, D. Wu, A. Lago, T. Devic, C. Martineau, F. Taulelle, P. L. Llewellyn, H. Jobic, C. Zhong, C. Serre, G. De Weireld, G. Maurin, *Angew. Chem. Int. Ed.*, **2013**, 52,
- [43] J. Liu, J. Tian, P. K. Thallapally, B. P. McGrail, *J. Phys. Chem. C*, **2012**, 116(17):9575 – 9581.
- [44] S. C. Xiang, Y. B. He, Z. J. Zhang, H. Wu, W. Zhou, R. Krishna and B. L. Chen, *Nat. Commun.*, **2012**, 3, 954.
- [44] W. K. Lewis, E. R. Gilliland, R. Chertow, W. P. Cadogan, *Ind. Eng. Chem.*, **1950**, 42, 1319-1326.
- [45] B. K. Kaul, *Ind. Eng. Chem. Res.*, **1987**, 26, 928-933.
- [46] A. S. Joy, *Vacuum*, **1953**, 3, 254-278.
- [47] K. Berlier, J. Bougard, M. G. Olivier, *Meas. Sci. Technol.*, **1995**, 6, 107.
- [48] Y. Belmabkhout, M. Frère, G. De Weireld, *Meas. Sci. Technol.*, **2004**, 15, 848-858.
- [49] O. Kunz, R. Klimeck, W. Wagner, M. Jaeschke, GERG Technical Monographie 15 Fortschr.-Ber. VDI, VDI-Verlag, Düsseldorf, **2007**.
- [50] A. L. Myers, J. M. Prausnitz, *AIChE J.*, **1965**, 11, 121.
- [51] Serre, C.; Groves, J.A.; Lightfoot, P.; Slawin, A.M.Z.; Wright, P.A.; Stock, N.; Bein, T.; Haouas, M.; Taulelle, F.; Férey, *Chem. Mater.*, **2006**, 18, 1451-1457.

- [52] J. VandeVondele, M. Krack, F. Mohamed, M. Parrinello, T. Chassaing and J. Hutter, *Comput. Phys. Commun.*, **2005**, 167, 103.
- [53] J. VandeVondele and J. Hutter, *J. Chem. Phys.*, **2003**, 118, 4365.
- [54] G. Lippert, J. Hutter and M. Parrinello, *Theor Chem Acc*, 1999, 103, 124; (d) B. G. Lippert, J. H. Parrinello and Michele, *Mol. Phys.*, **1997**, 92, 477.
- [55] J.P. Perdew, Y. Wang, *Phys. Rev. B*, **1986**, 33, 8822.
- [56] J. VandeVondele, J. J. Hutter, *Chem. Phys.*, **2007**, 127, 114105.
- [57] S. Goedecker, M. Teter, J. Hutter, *Phys. Rev. B.*, **1996**, 54, 1703.
- [58] S. Grimme, J. Antony, S. Ehrlich, H. Krieg, *J. Chem. Phys.*, **2010**, 132, 154104.
- [59] R.S. Mulliken, *J. Chem. Phys.*, **1955**, 23, 1833.
- [60] W.J. Hehre, J.A. Ditchfield, J.A. Pople, *J. Chem. Phys.*, **1972**, 56, 2257.
- [61] A. K. Rappé, C. J. Casewit, K. S. Colwell, W. A. Goddard III, W. M. Skiff, *J. Amer. Chem. Soc.* **1992**, 114, 10024.
- [62] J. G. Harris, K. H. Yung, *J. Phys. Chem.*, **1995**, 99, 12021.
- [63] M. G. Martin, J. I. Siepmann, *J. Phys. Chem. B*, **1998**, 102, 2569.
- [64] Q. Yang, C. Zhong, *J. Phys. Chem. B*, **2006**, 110, 17776–17783.
- [65] D.-Y. Peng, D. B. Robinson, *Ind. Eng. Chem. Fundam.*, **1976**, 15, 59.
- [66] T. J. H. Vlugt, E. García-Pérez, D. Dubbeldam, S. Ban, S. Calero, *J. Chem. Theory Comput.*, **2008**, 4, 1107-1118.
- [67] G. D. Pirngruber, P. Raybaud, Y. Belmabkhout, J. Čejka, A. Zúkal, *Phys. Chem. Chem. Phys.*, **2010**, 12, 13534–13546.
- [68] P. Nachtigall, M. R. Delgado, D. Nachtigallova, C.O. Arean, *Phys. Chem. Chem. Phys.*, **2012**, 14, 1552–1569.

